AP-1 is a temporally regulated dual gatekeeper of reprogramming to pluripotency

Glenn J. Markov[a,b,1], Thach Mai[a,1,2], Surag Nair[c], Anna Shcherbina[d], Yu Xin Wang[a], David M. Burns[a], Anshul Kundaje[b,c], and Helen M. Blau[a,3]

[a]Baxter Laboratory for Stem Cell Biology, Stanford University School of Medicine, Stanford, CA 94305; [b]Department of Genetics, Stanford University, Stanford, CA 94305; [c]Department of Computer Science, Stanford University, Stanford, CA 94305; and [d]Biomedical Informatics, Stanford University, Stanford, CA 94305

Contributed by Helen M. Blau, May 7, 2021 (sent for review March 17, 2021; reviewed by Michael Karin and Haifan Lin)

Somatic cell transcription factors are critical to maintaining cellular identity and constitute a barrier to human somatic cell reprogramming; yet a comprehensive understanding of the mechanism of action is lacking. To gain insight, we examined epigenome remodeling at the onset of human nuclear reprogramming by profiling human fibroblasts after fusion with murine embryonic stem cells (ESCs). By assay for transposase-accessible chromatin with high-throughput sequencing (ATAC-seq) and chromatin immunoprecipitation sequencing we identified enrichment for the activator protein 1 (AP-1) transcription factor c-Jun at regions of early transient accessibility at fibroblast-specific enhancers. Expression of a dominant negative AP-1 mutant (dnAP-1) reduced accessibility and expression of fibroblast genes, overcoming the barrier to reprogramming. Remarkably, efficient reprogramming of human fibroblasts to induced pluripotent stem cells was achieved by transduction with vectors expressing SOX2, KLF4, and inducible dnAP-1, demonstrating that dnAP-1 can substitute for exogenous human OCT4. Mechanistically, we show that the AP-1 component c-Jun has two unexpected temporally distinct functions in human reprogramming: 1) to potentiate fibroblast enhancer accessibility and fibroblast-specific gene expression, and 2) to bind to and repress *OCT4* as a complex with MBD3. Our findings highlight AP-1 as a previously unrecognized potent dual gatekeeper of the somatic cell state.

reprogramming pluripotency | c-Jun | transcription factor | heterokaryon

The discovery of a means to reprogram somatic cells to pluripotent stem cells enabled an explosion of research in stem cell therapy, disease modeling, and the study of mechanisms of reprogramming (1–6). A major impediment to conversion between cell states entails overcoming the mechanisms that maintain a cell's transcriptional program (7). The loss of endogenous transcription factors (TFs) that establish cell identity improves the efficiency of reprogramming to induced pluripotent stem cells (iPSCs) from embryonic fibroblasts or mature B cells (6, 8). However, it remains unclear if endogenous factors play an active role in repressing the pluripotency circuitry. In neurons, Mytl1 acts to repress nonneuronal genetic programs, including lineage specifiers, proliferation genes, and the Notch and Wnt pathways (9). In reprogramming to pluripotency, current evidence favors an indirect function for endogenous factors in maintaining accessible chromatin of the starting cell type, wherein exogenous reprogramming factors are sequestered away from enhancers of pluripotent stem cells (6, 10). However, due to the heterogeneity inherent in iPSC reprogramming, a comprehensive understanding of the antagonism between the somatic and pluripotent state is lacking.

In order to identify barriers to reprogramming to pluripotency, we profiled the early dynamics of epigenomic activity in the efficient heterokaryon system of nuclear reprogramming (11, 12). Following fusion of human fibroblasts with an excess of mouse embryonic stem cells (ESCs), on average 70% of the resulting multinucleate heterokaryons activate human pluripotency genes *OCT4* and *NANOG* within 48 h (13). During this time period, the transcriptome progressively shifts from the fibroblast state toward the ESC state, enabling experiments designed to address mechanistic questions that can then be validated in iPSC reprogramming (14, 15).

Here, we define two temporally distinct functions of c-Jun/AP-1 in reprogramming to pluripotency. We combined a time course of RNA sequencing (RNA-seq), assay for transposase-accessible chromatin with high-throughput sequencing (ATAC-seq), and chromatin immunoprecipitation followed by sequencing (ChIP-seq) to reveal that a reduction in both c-Jun occupancy and chromatin accessibility is required for suppression of the endogenous fibroblast program. Long known as a potent transactivator (16–18), our loss-of-function experiments reveal that activator protein 1 (AP-1) also operates as a repressor of *OCT4*, a pivotal pluripotency regulator, in both heterokaryons and iPSCs. Remarkably, dominant negative AP-1 (dnAP-1) surmounts this barrier to reprogramming and efficiently replaces exogenous OCT4 to convert human fibroblasts to a pluripotent iPSC state. Mechanistically, our results resolve opposing findings regarding Mbd3 and AP-1 family members in reprogramming (6, 19–21) by recasting c-Jun/AP-1 as an Mbd3-dependent repressor. Our studies provide fresh insights into the unexpected dual role of AP-1 as a gatekeeper of the somatic cell state and barrier to reprogramming to pluripotency.

Results

Identification of AP-1 as an Early Transient Regulator in Nuclear Reprogramming. In order to identify the early response of fibroblasts to reprogramming, we used the heterokaryon system, in which human

Significance

Reprogramming of somatic cells holds tremendous therapeutic promise. Here we show that a key barrier to this process is a DNA binding protein named activator protein 1 (AP-1). We find that AP-1 acts sequentially to first maintain the somatic state by turning genes on and then to block the initiation of the new cellular program by acting as a repressor of gene transcription. Crucially, we were able to uncover this feature of AP-1 by using the heterokaryon system of reprogramming, in which human fibroblasts are fused to an excess of mouse embryonic stem cells to favor the induction of the embryonic stem cell program in the fibroblast.

Author contributions: G.J.M., T.M., D.M.B., A.K., and H.M.B. designed research; G.J.M., T.M., and Y.X.W. performed research; G.J.M., S.N., A.S., Y.X.W., and A.K. contributed new reagents/analytic tools; G.J.M., T.M., S.N., A.S., and Y.X.W. analyzed data; and G.J.M., T.M., S.N., A.S., D.M.B., A.K., and H.M.B. wrote the paper.

Reviewers: M.K., University of California San Diego; and H.L., Yale University School of Medicine.

The authors declare no competing interest.

[1]G.J.M. and T.M. contributed equally to this work.

[2]Present address: Juvena Therapeutics Inc., Palo Alto, CA 94304.

[3]To whom correspondence may be addressed. Email: hblau@stanford.edu.

This article contains supporting information online at https://www.pnas.org/lookup/suppl/doi:10.1073/pnas.2104841118/-/DCSupplemental.

Published June 4, 2021.

fibroblasts (hFibs) are fused to an excess of mouse embryonic stem cells (mESCs) forming heterokaryons with an average nuclear ratio of ~1:3 hFib to mESC nuclei (15). We assayed chromatin accessibility by ATAC-seq and gene expression by RNA-seq in fluorescence-activated cell sorting (FACS)-purified heterokaryons at four time points with replicates (*SI Appendix*, Fig. S1). We chose 0, 3, 16, and 48 h postfusion to represent the starting fibroblast, early, middle, and late stages of heterokaryon reprogramming, respectively (Fig. 1*A*). The 3- and 16-h time points represent critical junctions in the transcriptome profile (14). The 0-h time point represents the controls, which are fibroblasts fused to one another (homokaryon fusion control), fibroblasts cocultured with ESCs (coculture control), and fibroblasts alone. These conditions allowed us to control for the effects of fusion and paracrine signals.

We found that heterokaryon reprogramming is highly dynamic at the level of chromatin accessibility. A case in point is the human *LIN28A* pluripotency locus at which there were fibroblast-specific peaks that progressively lost accessibility, ESC-specific peaks that progressively gained accessibility, and peaks with transient loss and gain dynamics (Fig. 1*B*). To investigate cis regulatory drivers of accessibility trajectories genome-wide, we clustered patterns of differential ATAC-seq peaks that mapped to the human genome using the Dirichlet process Gaussian process mixture model (DPGP) (22), and found 14 significant clusters of ATAC-seq peaks (Fig. 1*C*). To interpret accessibility dynamics in the context of reprogramming from the starting fibroblast state toward the embryonic stem cell state, we mapped the ATAC-seq peaks in each of the clusters to histone modification-based combinatorial chromatin states as defined by Roadmap Epigenomics (23) for both cell types (Fig. 1*D*). In clusters 1 to 3, accessibility decreased consistent with a less active chromatin state signature in the end state (ESC), and in clusters 4 and 5, accessibility increased by 48 h postfusion in accordance with a higher proportion of active states in ESC chromatin (Fig. 1*D*). By contrast, the transient loss and transient gain trajectories (clusters 8 to 10 and 11 to 14, respectively, Fig. 1*C*) could not be predicted by examining the end states alone (Fig. 1*D*).

To identify regulators of these dynamic chromatin states, we quantified the transcription factor motif enrichment for all the trajectories (24). Transcription factor motifs showed strong coenrichment by several distinct groupings (*SI Appendix*, Fig. S2). Representatives of these motif families are summarized in Fig. 1*E*. Notably, AP-1 was the most enriched motif in the transient gain clusters 11 to 14 (*SI Appendix*, Fig. S3*A*). Taken together, heterokaryon reprogramming enabled identification of distinct chromatin accessibility trajectories with unique combinations of transcription factor motifs, which define an epigenomic roadmap for somatic cell reprogramming to pluripotency.

c-Jun Acts Early to Promote Fibroblast Gene Expression. We sought to examine the role of factors driving an early transient gain in accessibility in fibroblasts undergoing heterokaryon reprogramming that might be missed in a time course of heterogenous iPSC induction. To that end, we investigated the canonical AP-1 (Jun/Fos) family members, which share the binding motif enriched in clusters 11 to 14 (24) (Fig. 1*E*). By gene expression, all seven Jun/Fos homologs peaked in the first 2 h of the 24-h time course. *FOS*, *FOSB*, *JUN*, and *JUNB* exhibited the earliest response with expression peaking at 0.5 h postfusion, whereas expression of *FOSL1*, *FOSL2*, and *JUND* peaked at 2 h (*SI Appendix*, Fig. S3*B*). In contrast, *BACH1*, *JDP2*, and *PAX8* did not exhibit the same striking expression kinetics or absolute expression values, even though their motifs were coenriched in the same clusters (*SI Appendix*, Fig. S3*C*). Both c-Jun and Fosl1 have been implicated in iPSC reprogramming (10, 21). Since both Jun and Fos family dimers must contain a Jun family member (25, 26), we investigated the genome-wide occupancy of c-Jun using the recently developed high-throughput ChIPmentation approach (27), which enables an increase in library complexity by reducing the steps in the standard ChIP-seq protocol. We found that regions occupied by c-Jun had a very robust enrichment for the canonical AP-1 binding motif (*SI Appendix*, Fig. S3*D*) and a high degree of concordance with accessible regions by ATAC-seq in the starting human fibroblast line (Fig. 1*F*). Since c-Jun has been implicated in promoting the epithelial–mesenchymal transition (EMT), we examined 130 genes that had been determined in a metaanalysis to have consistent up-regulation (EMTup) or down-regulation (EMTdown) during EMT (28). We found that EMTup genes mirrored the transient up-regulation of *JUN* mRNA expression, including potent positive regulators *TWIST2* and *ETS1* (29, 30) (*SI Appendix*, Fig. S3 *E–G*). Conversely, EMTdown genes were gradually up-regulated during the time course (*SI Appendix*, Fig. S3*E*).

In the chromatin-state analysis (Fig. 1*D*), clusters 11 to 14 had strong enrichment in both occurrences of the AP-1 motif and fibroblast enhancers compared to a relative depletion of hESC enhancers. We tested this dichotomy further by comparing the presence of the active enhancer mark H3K27ac in both fibroblasts and hESCs at genomic regions occupied by c-Jun. In fibroblasts, but not in hESCs, the active enhancer-associated histone mark H3K27ac flanks c-Jun sites (Fig. 2*A*). We further performed gene ontology (GO) term enrichment using GREAT (31), which maps genomic regions to proximal genes. We found a number of enrichments for functions and pathways in fibroblasts, which included genes related to extracellular matrix, growth signaling, and migration (*SI Appendix*, Fig. S4). c-Jun bound genes in these enriched GO categories had significantly higher expression in fibroblasts than in hESCs, suggesting c-Jun activity maintains a fibroblast chromatin state (Fig. 2*B* and *SI Appendix*, Table S1 and S2).

To perturb c-Jun function while minimizing effects of compensation by related family members, we used a dominant negative inhibitor of AP-1 (dnAP-1). The inhibitor encodes the c-Fos leucine zipper heterodimerization region with an extension of acidic residues that interact and interfere with the positively charged DNA binding domain of Jun family members (32). The high-affinity interaction disrupts formation of the endogenous AP-1 complex and blocks binding of AP-1 to DNA (Fig. 2*C*). To control the timing of expression of dnAP-1, we used a doxycycline (dox)-inducible system to express dnAP-1 as a fusion protein with RFP, separated by a cleavable linker so that function is minimally impacted. By flow cytometry, RFP signal was clearly detected at 12 h after dox addition and continued to increase at 24 h (*SI Appendix*, Fig. S5*A*). Functionally, dnAP-1 expression down-regulated known AP-1 target genes *FOSL1* and *SERP1* (*SI Appendix*, Fig. S5 *B* and *C*). We induced dnAP-1 in fibroblasts prior to fusion and analyzed chromatin accessibility in FACS-purified heterokaryons by ATAC- and RNA-seq. A marked decline in accessibility was observed at c-Jun-bound AP-1 sites at 3 h postfusion (Fig. 2*D*), but not at control ATAC-seq peaks without an AP-1 site or at sites containing the CTCF binding motif (*SI Appendix*, Fig. S5 *D* and *E*). These data provide strong evidence that c-Jun is a potent regulator of chromatin accessibility.

We sought to examine the link between c-Jun occupancy and chromatin accessibility on genes expressed in fibroblasts, but not embryonic stem cells ("fibroblast genes") early in reprogramming. We compared expression of fibroblast genes at 3 h postfusion with and without dnAP-1 and used the set of fibroblast genes that were not bound by c-Jun and did not exhibit a loss of chromatin accessibility with dnAP-1 induction as controls. Compared with this gene set, induction of dnAP-1 resulted in a mild down-regulation of gene expression at genes bound by c-Jun that did not lose chromatin accessibility (−0.04 mean fold change) and at genes not bound by c-Jun, which did lose chromatin accessibility (−0.12 mean fold change) (Fig. 2*E*). Genes that are targeted by c-Jun, but do not exhibit decreased accessibility, may have compensatory mechanisms that regulate their chromatin accessibility. Importantly, there was a significant and striking loss of expression of fibroblast genes which 1) bound c-Jun in the somatic cell state

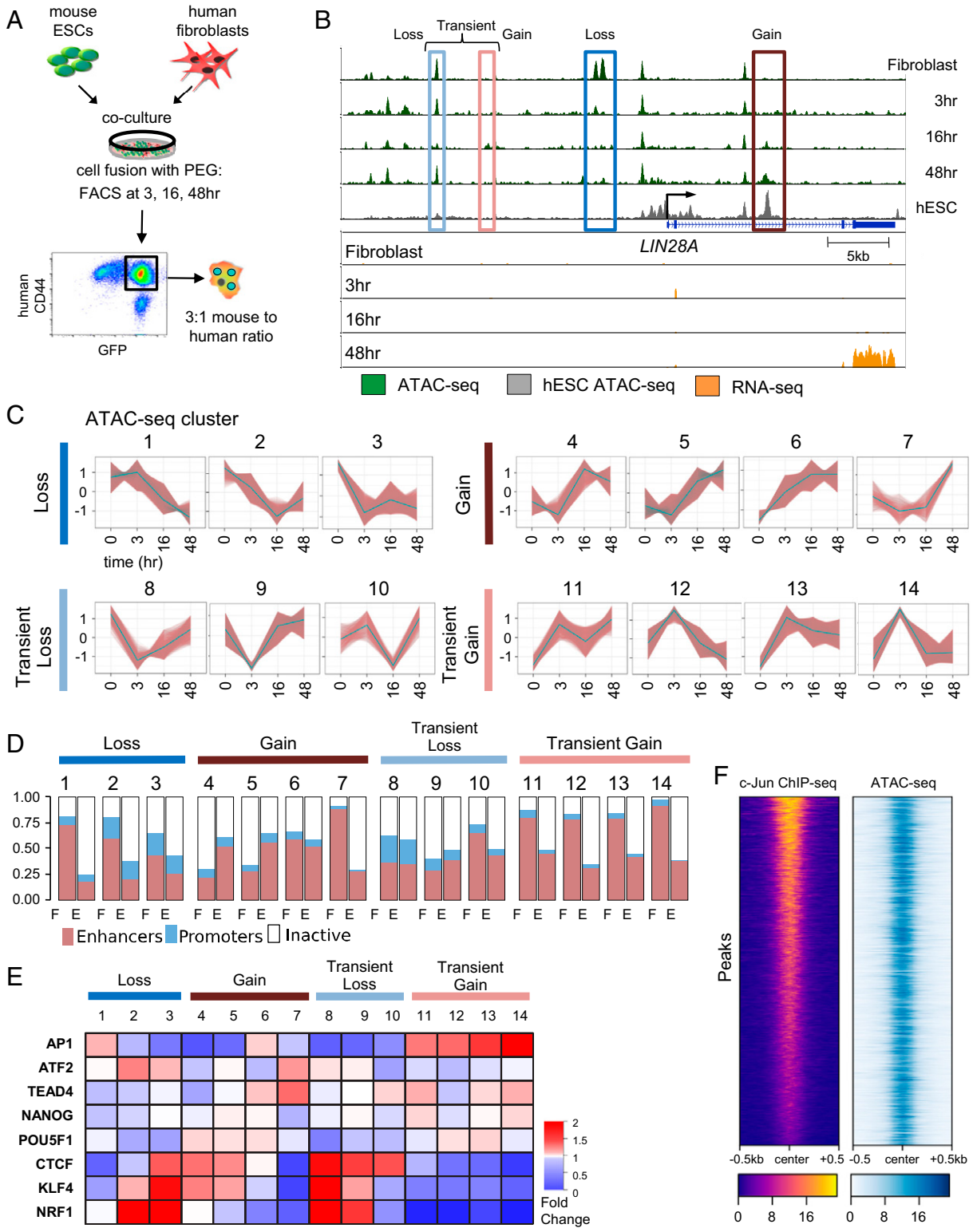

Fig. 1. Chromatin accessibility dynamics during heterokaryon reprogramming. (*A*) Experimental setup: GFP$^+$ mouse ESCs fused to human fibroblasts and sorted at 3, 16, and 48 h postfusion. (*B*) Human *LIN28A* locus with ATAC-seq and RNA-seq tracks. (*C*) Differentially accessible ATAC-seq peaks clustered and classified into four patterns. (*D*) Chromatin states in the starting fibroblast (F) and ending ESC (E) cell types for each cluster of genomic regions (*C*). (*E*) Heatmap of transcription factor motif enrichment for ATAC-seq clusters (*C*). (*F*) c-Jun ChIP-seq and ATAC-seq signal in human fibroblasts at c-Jun binding sites ranked from most to least (top to bottom) signal in the ChIP-seq track.

and 2) exhibited loss of chromatin accessibility after dnAP-1 induction (−0.78 mean fold change, $P < 0.001$) (Fig. 2*E*). These analyses suggest that c-Jun plays an important role in promoting chromatin accessibility and fibroblast gene expression in both homeostasis and in the early, transient phase of reprogramming to pluripotency.

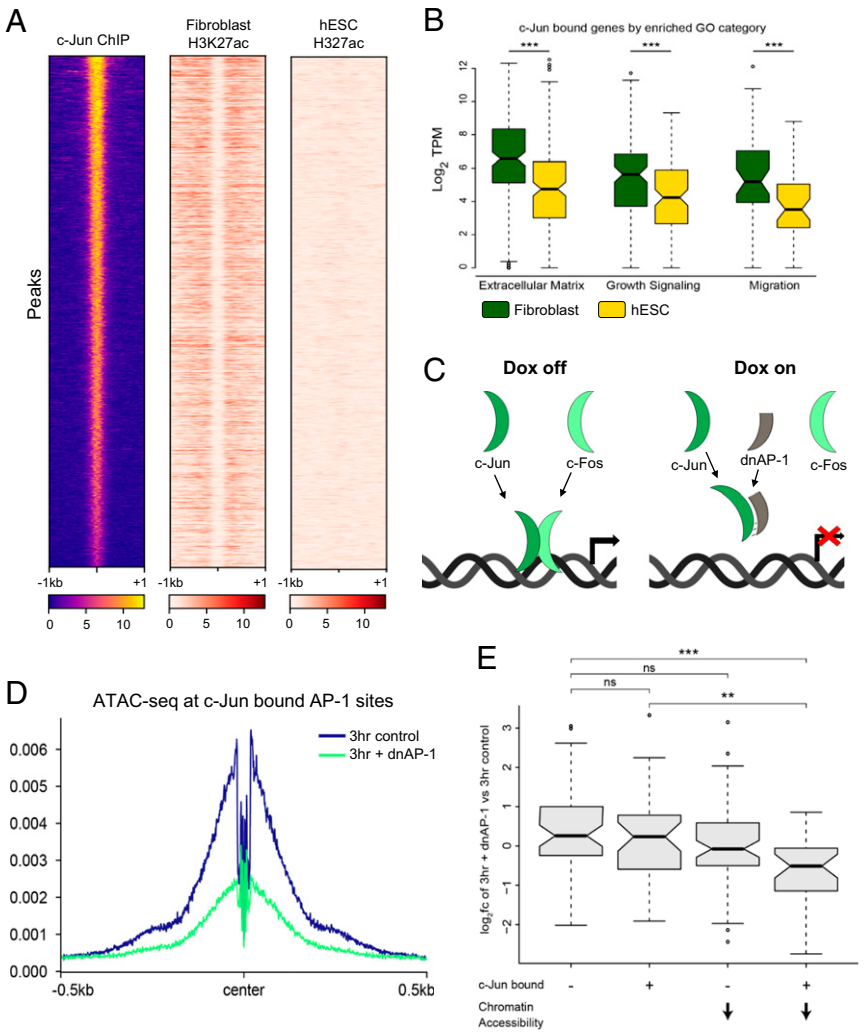

Fig. 2. AP-1 regulates fibroblast-specific gene expression early in reprogramming. (*A*) Heatmaps of c-Jun ChIP-seq, IMR90 fibroblast H3K27ac, and H1 hESC H3K27ac signal ranked by most to least signal c-Jun ChIP-seq signal. The H3K27ac datasets are from the Roadmap Epigenomics Project. (*B*) Gene expression captured by RNA-seq and plotted as $\log_2$ transformed transcripts per million (TPM) for three GO term–derived gene groupings. *P* values calculated using the Wilcoxon rank-sum test with Holm–Sidak correction ($n > 40$). (*C*) Schematic illustrating mechanism of dnAP-1 acting to inhibit AP-1 activity. (*D*) ATAC-seq footprint with or without dnAP-1 induction at c-Jun occupied peaks in heterokaryons at 3 h postfusion centered at AP-1 motif (TGA G/C TCA). (*E*) Expression of fibroblast genes in heterokaryons 3 h postfusion after induction of dnAP-1. Gene subsets with a c-Jun binding site within 20 kb of their TSS are denoted as c-Jun bound (+). Gene subsets with a significant loss of chromatin accessibility are denoted with a down arrow. Comparisons were performed using a one-way ANOVA with Sidak's multiple comparisons test ($n > 30$). For plots in *B* and *E*, the box boundaries represent the first and third quartile and the center line is the median. Outliers outside of the 1.5× interquartile range of the whiskers are plotted as individual points. ns ($P > 0.05$), $^{**}P < 0.01$, $^{***}P < 0.001$.

c-Jun Inhibits Activation of *OCT4*. To test the function of AP-1 in nuclear reprogramming, we measured expression levels of pluripotency genes 48 h after induction of dnAP-1 (Fig. 3*A*). There was a significant increase in human *OCT4* mRNA at 48 h, even when dnAP-1 was induced postfusion (Fig. 3*B*). Moreover, human *OCT4* mRNA expression was up-regulated just 16 h postfusion (Fig. 3*C*). These results suggest AP-1 plays a role early as well as late in reprogramming. Given our previous demonstration that 70% of heterokaryons express human *OCT4* and *NANOG* by 48 h postfusion (13), the fourfold increase in human *OCT4* mRNA must be due to up-regulation of *OCT4* expression, rather than an increase in the number of cells expressing *OCT4*. Additionally, pluripotency genes *NANOG* and *LIN28A* had elevated expression on average after dnAP-1 induction (*SI Appendix*, Fig. S5 *F* and *G*). As *NANOG* and *LIN28A* are OCT4 target genes, there may be additional regulatory steps between AP-1 activity and their gene expression (33–35). Moreover, the transient peaks of chromatin accessibility near *LIN28A* (Fig. 1*B*) do not harbor the canonical AP-1 motif and do not exhibit detectable c-Jun occupancy, suggesting they are not directly regulated by c-Jun. For these reasons, we focused on the activation of *OCT4*.

To dissect the regulation of *OCT4* activation, we targeted catalytically inactive Cas9 (dCas9) fused to the KRAB repressor domain to accessible sites identified by ATAC-seq near the *OCT4* locus in human fibroblasts prior to heterokaryon formation. Repression by dCas9-KRAB does not extend beyond the flanks of the accessible site targeted (36), but can silence gene expression via looping (37). We designed guide RNAs targeted to six regions, which included two AP-1 motif-containing accessible regions (AP1r1 and AP1r2), an intronic accessible region present in naïve hESCs (38) and heterokaryons, proximal and distal enhancer regions previously identified (38), and the transcription start site (TSS) as a control (*SI Appendix*, Fig. S6*A*). With the exception of the element near the 3′ UTR (AP1r1), all of the regulatory regions tested showed

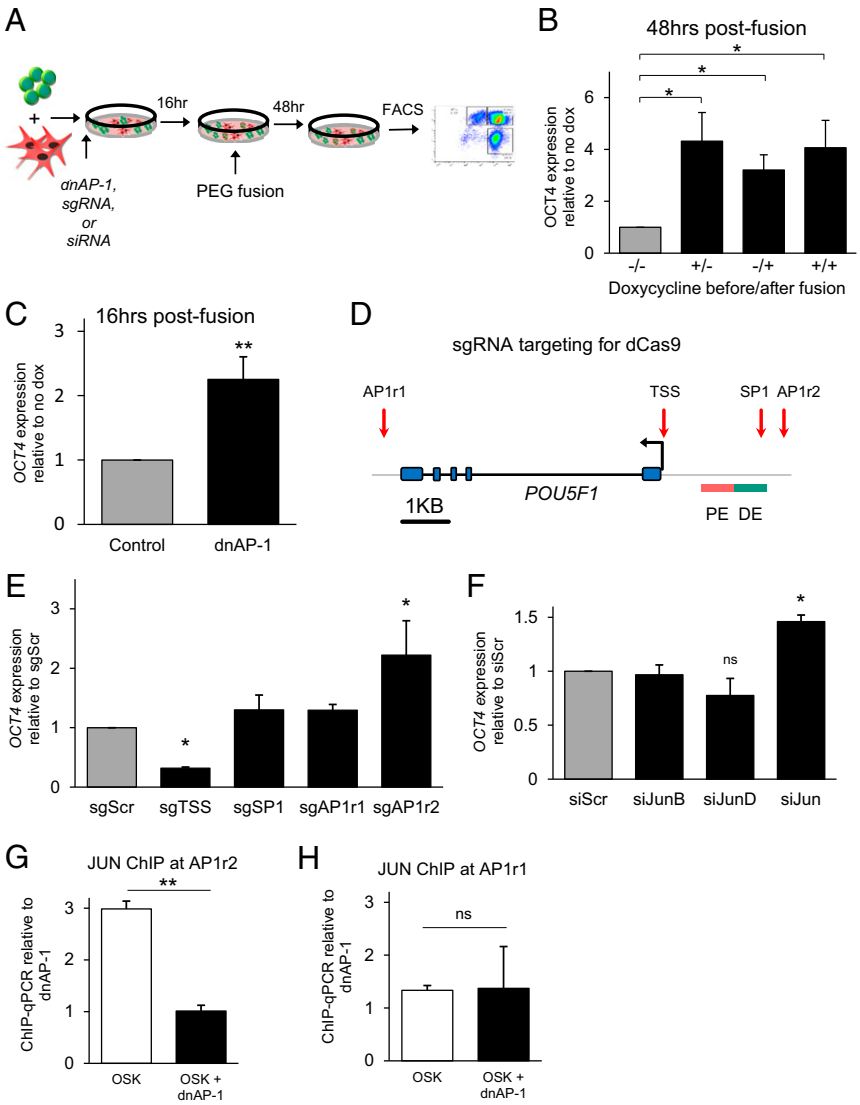

Fig. 3. c-Jun inhibits *OCT4* expression during reprogramming. (*A*) Experimental setup for heterokaryon perturbation experiments where cells are treated at the start of the overnight coculture period and then sorted 48 h postfusion. (*B*) Human *OCT4* gene expression by qRT-PCR in heterokaryons following induction of dominant negative AP-1 with $n = 3$ biological replicates. (*C*) Same as in *B* except assayed at 16 h postfusion with $n = 5$ biological replicates. (*D*) Diagram of dCas9 sgRNA sites. DE and PE are distal and proximal enhancer, respectively. (*E*) Human *OCT4* levels in heterokaryons expressing catalytically inactive Cas9 (dCas9) and the listed sgRNA ($n = 3$ to 5 biological replicates). (*F*) Human *OCT4* expression in heterokaryons after delivery of siRNA against the mouse and human mRNA of the gene listed, plotted relative to sample receiving siScr ($n = 3$ to 4 biological replicates). *B*, *C*, *E*, and *F* were calculated with a one-sample two-tailed *t* test for the conditions indicated. (*G* and *H*) ChIP-qPCR of c-Jun in human fibroblasts 8 d posttransduction with vectors expressing *OCT4*, *SOX2*, and *KLF4* (OSK). Data were normalized to input and plotted relative to the fibroblasts which had dnAP-1 induced for 24 h prior to harvest (negative control for c-Jun binding). ChIP location is shown in *D*; $n = 3$ biological replicates, two-tailed Student's *t* test. ns ($P > 0.05$), $*P < 0.05$, $**P < 0.01$.

a >50% reduction in *OCT4* gene expression, suggesting these elements may interact with and regulate the *OCT4* locus (*SI Appendix*, Fig. S6*B*).

To test if AP-1 family members target *OCT4* through specific motifs at the regulatory regions described above (*SI Appendix*, Fig. S6*A*), we employed dCas9 lacking the KRAB domain. dCas9 has been shown to block TF function when targeted to the TF binding site (39). We targeted the AP-1 motif (TGA G/C TCA) and the SP1 motif at accessible genomic elements near *OCT4* (Fig. 3*D*). The SP1 motif was targeted based on prior studies demonstrating AP-1 can act at an SP1 binding site via a physical interaction between c-Jun and SP1 factors (16, 40). Coexpressing dCas9 with a guide RNA targeting the TSS significantly decreased *OCT4* gene expression at 48 h in heterokaryons as expected (Fig. 3*E*). In contrast, blocking the AP-1 site at AP1r2 significantly increased *OCT4* expression (Fig. 3*E*). This finding is consistent with the hypothesis that AP-1 acts to inhibit *OCT4* transcription at least in part via AP1r2.

c-Jun Inhibits *OCT4* via Upstream Regulatory Element. To dissect how individual AP-1 family members regulate the pluripotency network, we targeted Jun, JunB, or JunD mRNAs with siRNA in heterokaryons. Jun family proteins can form homodimers, whereas Fos family proteins depend on the Jun family to form heterodimers and bind DNA. Although the human transcripts are more abundant, we designed siRNAs against transcripts of both species (*SI Appendix*, Table S3). Knockdown efficiencies were similar for all three Jun family members for the human and mouse transcripts (*SI Appendix*,

Fig. S7 *A* and *B*). Knockdown of JunB or JunD did not significantly alter *OCT4* expression in heterokaryons (Fig. 3*F*). By contrast, siRNA against Jun resulted in an increase in *OCT4* expression ($P < 0.05$) (Fig. 3*F*).

The increase in *OCT4* after siJun treatment together with the dCas9 targeting experiment (Fig. 3*E*) suggested that c-Jun acts to repress *OCT4* via AP1r2. To test c-Jun occupancy at this element, we performed ChIP-qPCR with or without dnAP-1 induction in human fibroblasts transduced with iPSC reprogramming factors, as cell numbers were limiting for accurate transcription factor ChIP-qPCR in heterokaryons. As expected, there was significant signal at the *JUN* promoter, as c-Jun has previously been reported to be autoregulatory (17) (*SI Appendix*, Fig. S7*C*). Importantly, c-Jun showed an enrichment at the AP1r2 site upstream of *OCT4* relative to cells where dnAP-1 was induced (Fig. 3*G*) in contrast to AP1r1 (Fig. 3*H*) in corroboration with the dCas9 experiment showing that AP-1 occupies this site in reprogramming fibroblasts (Fig. 3*E*).

c-Jun and MBD3 Interact during Nuclear Reprogramming. We postulated that an interaction between c-Jun and a repressor could result in c-Jun–mediated inhibition of *OCT4* expression during reprogramming. A yeast three-hybrid screen for proteins that interact with c-Jun has previously identified MBD3, a member of the NuRD-repressor complex (41). We tested if there was an enrichment in occupancy of MBD3 at the AP1r1 and AP1r2 regions in human fibroblasts undergoing iPSC reprogramming by ChIP in the presence or absence of dnAP-1. We found a significant enrichment of AP-1–dependent MBD3 binding at AP1r2, but not at AP1r1 (Fig. 4 *A* and *B*), suggesting that MBD3 may be recruited by an AP-1 family member to AP1r2.

The possibility of a physical association prompted us to test if c-Jun and Mbd3 interact during reprogramming. We used the proximity ligation assay (PLA) in heterokaryons in which the mouse ESCs contained a FLAG tag knocked into the *Mbd3* locus (42) (Fig. 4*C*). We detected the interaction between c-Jun and MBD3 in heterokaryons at 2, 16, and 48 h postfusion with anti–c-Jun and anti-FLAG antibodies, using *Mbd3* knockout (KO) cells from the same time point as controls (Fig. 4*D* and *SI Appendix*, Fig. S7*D*). The frequency of the interaction was highly significant at all three time points (Fig. 4*E*). Furthermore, the interaction frequency was higher at 16 and 48 h postfusion (37 and 33%, respectively) compared to 2 h (4.6%) (Fig. 4*E*). This finding was confirmed by coimmunoprecitiation (co-IP) as detailed in Fig. 4. These results strongly suggest that the physical interaction between c-Jun and Mbd3 described in vitro (41) also occurs in vivo during heterokaryon reprogramming.

To test if the inhibition of *OCT4* by c-Jun can be overcome by the loss of MBD3 in heterokaryons, we overexpressed c-Jun in the presence of siMbd3, targeting both mouse and human transcripts or a scrambled siRNA. The reduction of *Mbd3* mRNA by siRNA was validated (*SI Appendix*, Fig. S7 *E* and *F*). A significant reduction in *OCT4* expression was seen in heterokaryons when c-Jun was overexpressed ($P < 0.05$) (Fig. 4*F*). This decrease in *OCT4* expression was rescued by codelivery of siRNA against *Mbd3* mRNA, suggesting *OCT4* expression is negatively regulated by c-Jun through its interaction with MBD3 (Fig. 4*F*).

Temporal Regulation of c-Jun Activity by Phosphorylation. The c-Jun–MBD3 interaction in a cell lysate can be abrogated by phosphorylation of c-Jun at the transactivation domain (41). To explore the dynamics of c-Jun phosphorylation in intact cells in vivo, we measured phospho-c-Jun (pJun) levels relative to total c-Jun by flow cytometry in reprogramming heterokaryons over several time points. The ratio of pJun to c-Jun increased transiently at 2 h postfusion ($P < 0.05$) (Fig. 5 *A* and *B*). The high levels of pJun early and subsequent decline (Fig. 5*B*) are consistent with a lower frequency of the c-Jun–MBD3 interaction at 2 h compared to 16 and 48 h postfusion as assayed by PLA (Fig. 4*E*). To test if the inhibitory function of c-Jun in reprogramming is phosphorylation dependent, we measured *OCT4* mRNA in heterokaryons after expression of JNK1 fused to Mkk7 to create a constitutive JNK (cJNK) (43). c-Jun is a well-characterized target of JNK1 (also known as MAPK8) (44), and JNK1 is a target of Mkk7 (45). As controls, we used the same construct with mutations at the catalytic site of JNK1 (cJNKmut) and a construct expressing mCherry. Expression of cJNK increased both intracellular levels of pJun (*SI Appendix*, Fig. S8) and *OCT4* expression ($P < 0.05$) (Fig. 5*C*), suggesting that unphosphorylated c-Jun inhibits *OCT4* expression.

To determine if the phosphorylated residues are critical for the c-Jun–MBD3 interaction, we expressed HA-tagged c-Jun mutants with substitutions at the serine and threonine residues in the transactivation domain to either alanine (phospho-null) or aspartic acid (phosphomimetic) (46) (Fig. 5*D*). IP for HA followed by Western blot for c-Jun confirmed high expression and successful IP (Fig. 5*E*). In the same lysates, an interaction with MBD3 was apparent by co-IP with the alanine mutant, but not with the aspartic acid mutant (Fig. 5*F*), consistent with previous findings that the negatively charged phospho residues on in vitro phosphorylated recombinant c-Jun block its interaction with MBD3 (41).

Taken together, these results support a dynamic model wherein c-Jun function changes in the course of reprogramming: from steady-state maintenance of fibroblast function to a highly active phosphorylated form early in reprogramming, and then to an unphosphorylated form that interacts with Mbd3 to inhibit *OCT4* activation (Fig. 5*G*).

Role of AP-1 in iPSC Reprogramming. We postulated that our findings in heterokaryons could be applied to reprogramming fibroblasts to iPSCs. We capitalized on our finding that inhibition of AP-1 activity increases *OCT4* expression during nuclear reprogramming (Fig. 3 *B* and *C*) and the finding by others that truncated c-Jun can replace OCT4 in mouse iPSC reprogramming (21) to test if dnAP-1 could substitute for exogenous OCT4 in human iPSC reprogramming. We designed an OCT4 replacement experiment in which each reprogramming factor was expressed by a single retrovirus. MYC was omitted because it is not necessary for reprogramming (47) and can lead to partially reprogrammed colonies (48). In conjunction with constitutive expression of KLF4 and SOX2, dominant negative AP-1 was induced either early and transiently, late transiently, late constitutively, or throughout (Fig. 6*A*). We found that transient inhibition of endogenous AP-1 was sufficient to replace exogenous OCT4 and resulted in $NANOG^+$ iPSC colonies, whether the inhibition was early or late (Fig. 6 *B* and *C*). Overall the efficiency was highest when dnAP-1 was expressed throughout the time course, in support of a temporally regulated dual role for AP-1 in reprogramming (Fig. 6*B*). Notably, the efficiency of iPSC reprogramming in the continuous presence of dnAP-1in lieu of exogenous OCT4 exceeded that of the control (Fig. 6*B*).

We clonally selected and expanded iPSC colonies and profiled them by RNA-seq. Pairwise comparisons of gene expression revealed similar transcriptional profiles between OSK and SK + dnAP-1 iPSCs, and divergent profiles between the starting fibroblasts and SK + dnAP-1 iPSCs (Fig. 6*D*). The SK + dnAP-1-derived iPSCs expressed standard markers of pluripotency NANOG, OCT4, SOX2, and TRA-1-60 after selection and remained positive for these pluripotency proteins after expansion and passaging in culture (Fig. 6*E* and *SI Appendix*, Fig. S9).

Discussion

Our studies uncover an unexpected role for the widely known transactivator, c-Jun, as a potent roadblock that must be surmounted for nuclear reprogramming to iPSCs to occur. c-Jun acts as a barrier to reprogramming to pluripotency via two temporally distinct mechanisms. Early in reprogramming, c-Jun functions transiently to drive fibroblast

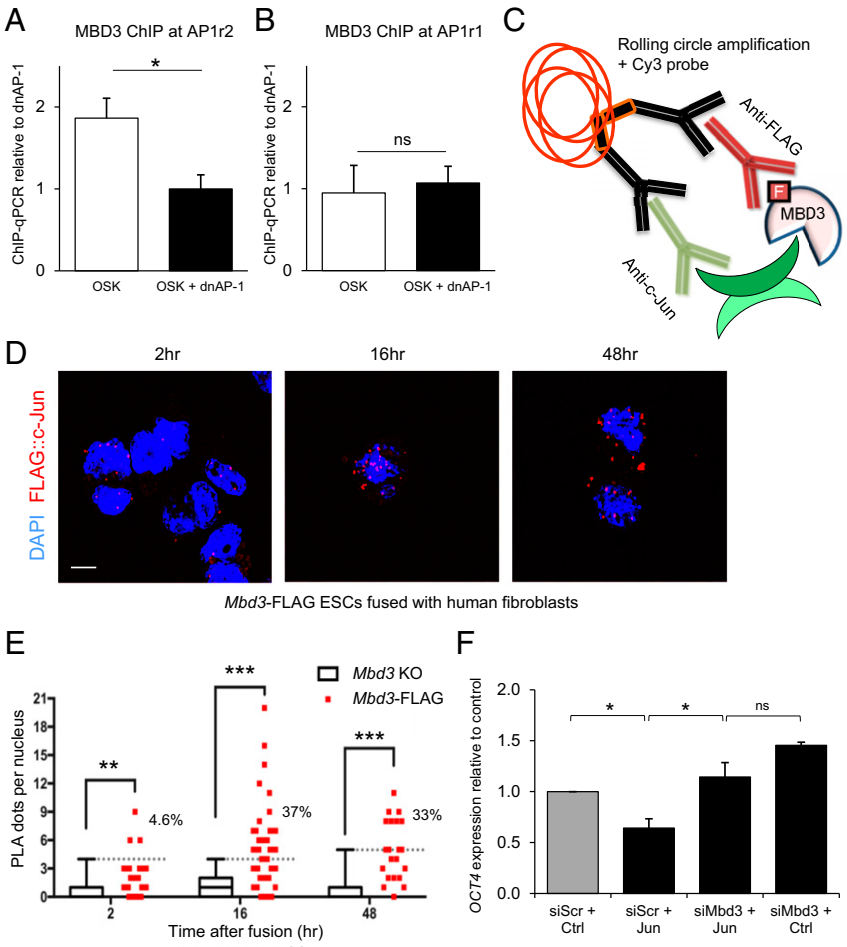

Fig. 4. Interaction between c-Jun and MBD3 during heterokaryon reprogramming. (*A* and *B*) ChIP-qPCR of MBD3-FLAG in human fibroblasts 8 d posttransduction with OSK and MBD3-FLAG. Data were normalized to input and plotted relative to the condition with dnAP-1; $n = 3$ biological replicates, two-tailed Student's *t* test. (*C*) Diagram of the PLA experimental design (*D* and *E*). (*D*) Proximity ligation assay between c-Jun and FLAG-MBD3 in heterokaryons. Representative image at each time point is shown. (Scale bar, 20 μM.) (*E*) Interactions from *D* that were overlapping DAPI signal were scored and quantified. $n > 30$ nuclei were quantified per time point, comparisons made with two-tailed Student's *t* test. (*F*) Human *OCT4* gene expression in heterokaryons at 48 h postfusion following codelivery of an expression vector and an siRNA against either *Mbd3* mRNA (mouse and human) or a scrambled control. Two-tailed Student's *t* test was performed on the comparisons indicated; $n = 4$ biological replicates. ns ($P > 0.05$), $^{*}P < 0.05$, $^{**}P < 0.01$, $^{***}P < 0.001$.

chromatin accessibility and gene expression. Later in reprogramming, c-Jun represses the pluripotency master regulato *OCT4*.

Our findings provide strong support that c-Jun/AP-1 is a major regulator of the fibroblast state, which has therapeutic implications. Expression of an inducible dominant negative AP-1 mutant (dnAP-1) disrupts chromatin accessibility at c-Jun–bound AP-1 sites. Crucially, a majority of c-Jun targets that exhibit a loss of chromatin accessibility following induction of dnAP-1 are genes expressed in fibroblasts, but not embryonic stem cells. These data provide insight into the epigenetic memory of the somatic cell that has been postulated to impede reprogramming (6, 10) and may in part explain defects specific to iPSC differentiation, which are not found in ESC differentiation (49, 50). Additionally, our findings have important implications for therapeutic interventions for fatal diseases caused by fibroblast-mediated scarring, such as idiopathic pulmonary fibrosis. Indeed, c-Jun overexpression has been shown to be sufficient to drive the disease via downstream targets, including inflammatory cytokines, immune checkpoints, and secreted collagens (51, 52). c-Jun/AP-1 has also been demonstrated to act in concert with BAF and cell type–specific transcription factors to regulate chromatin accessibility and gene expression in diverse cell types such as T cells, fibroblasts, and neurons (53). Our findings that early transient dnAP-1 expression can disrupt fibroblast chromatin accessibility and gene expression suggest that this strategy for resetting the AP-1–dependent somatic cell epigenome could prove useful therapeutically in countering pathologic fibrosis.

Previously, c-Jun was hypothesized to function indirectly to inhibit pluripotency genes (21). This was based on the use of a truncated c-Jun that increased the efficiency of iPSC reprogramming (21). However, the interpretation of these studies was confounded by the use of a mutant c-Jun that not only lacks the transactivation region but also the Mbd3 interaction domain (41). In contrast, here we dissociate these two properties by showing that 1) in its unphosphorylated state, c-Jun's transactivation domain is crucial to its complex formation with Mbd3; and 2) this complex binds to a previously unrecognized regulatory region near the *OCT4* distal enhancer, which represses the expression of the pluripotency master regulator *OCT4*. Although this complex has been reported in a colon cancer cell line (41), to our knowledge AP-1 has not previously been shown to interact with Mbd3 in the context of nuclear reprogramming to iPSCs.

Our model provides fresh insight into the controversial role of Mbd3 in iPSC reprogramming. Studies showed that *Mbd3*

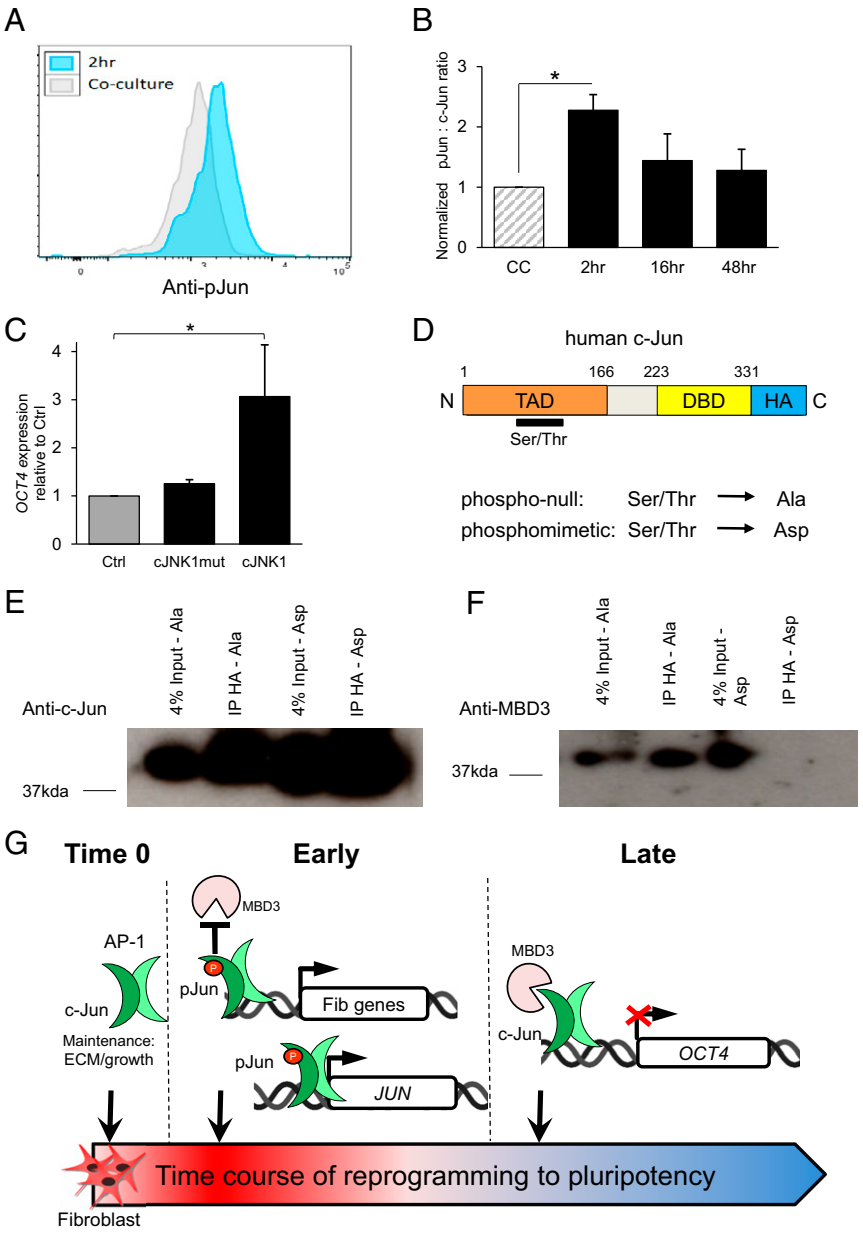

Fig. 5. Phosphorylation of c-Jun blocks interaction with MBD3 and activates *OCT4*. (*A*) Phosphoflow with anti-phospho c-Jun (pJun) in heterokaryons at 2 h postfusion vs. coculture control. (*B*) Quantified phospho-flow data for anti-pJun vs. anti–c-Jun shown as mean ± SEM relative to coculture (CC). Comparison made with one sample two-tailed *t* test ($n = 3$ biological replicates). (*C*) Human *OCT4* gene expression in heterokaryons after delivery of a vector encoding mCherry (Ctrl), catalytically inactive JNK fused to Mkk7 (cJNK1mut), or JNK fused to Mkk7 (cJNK1). Comparison made with one sample two-tailed *t* test ($n = 5$ biological replicates). (*D*) Diagram of human c-Jun constructs used in *E* and *F*, including the HA-tag, DNA binding domain (DBD), and the location of mutated serine/threonine residues in the transactivation domain (TAD). (*E* and *F*) Western blot from samples expressing one of two HA-tagged c-Jun mutants. Samples are 4% input or anti-HA IP. Blot is probed either anti-c-Jun (*D*) or anti-MBD3 (*F*). (*G*) Model of c-Jun as a barrier to reprogramming to pluripotency. $*P < 0.05$.

knockdown in reprogramming fibroblasts increases iPSC colony numbers (54) and the percentage of Nanog-GFP$^+$ cells during iPSC reprogramming (19). In contrast, another study reported that MBD3 loss decreases iPSC colony numbers when the starting cell type is an epiblast stem cell or a neural precursor (20). We postulate that the effects of Mbd3 loss of function in reprogramming are cell context dependent due to the AP-1/MBD3 complex, which reconciles these disparate findings. Specifically, cell type differences in c-Jun levels will determine whether loss of Mbd3 promotes or inhibits iPSC generation. Indeed, fibroblasts have high levels of c-Jun (55), while epiblast cells have low levels of c-Jun (56). Consistent with our hypothesis, loss of Mbd3 increased expression of pluripotency genes *Zfp42* (also known as *Rex1*) and *Klf5* in a liver cancer stem cell model in which c-Jun and Mbd3 co-occupy AP-1 sites at the *Zfp42* and *Klf5* promoters (57). Taken together, our findings suggest there are temporally distinct Mbd3-dependent and -independent mechanisms of action for AP-1 as a barrier to reprogramming to pluripotency.

Methods

See detailed methods in *SI Appendix*.

Heterokaryon Generation and Isolation. Human MRC-5 fibroblasts (ATCC CCL-171) were cultured in 10% fetal bovine serum (FBS) and Dulbecco's Modified

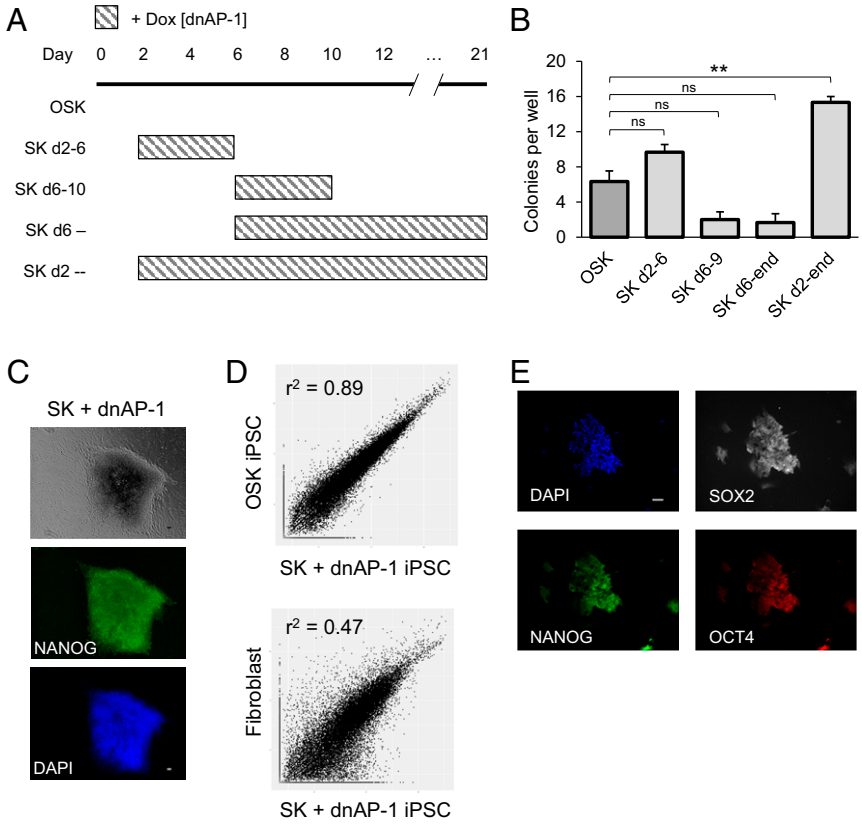

Fig. 6. Inhibition of AP-1 augments mouse and human iPSC induction. (*A*) Schematic for induction of dnAP-1 during iPSC reprogramming. (*B*) Quantification of NANOG$^+$ iPSC colonies. *P* values were calculated using a one-way ANOVA with Dunnett's multiple comparisons test; $n = 3$ biological replicates. (*C*) Representative human iPSC colony in phase contrast and by immunofluorescence with anti-NANOG staining. (Scale bar, 100 μm.) (*D*) Pairwise transcriptome-wide gene expression scatterplots of the OSK and SK + dnAP-1–derived iPSCs (*Top*) and the SK + dnAP-1 and the starting fibroblasts (*Bottom*). (*E*) Immunofluorescence of passaged iPSCs derived from reprogramming with vectors constitutively expressing *SOX2*, *KLF4*, and transiently expressing dnAP-1 for days 2 to 6. ns ($P > 0.05$), $^{**}P < 0.01$. (Scale bar, 20μm.)

Eagle Medium (DMEM). Generation of heterokaryons by cell fusion is described previously (13, 15).

ATAC-Seq Library Generation. ATAC-seq libraries were prepared as described (14).

ATAC-Seq and RNA-Seq Mapping and Quantification. RNA-seq and ATAC-seq reads were mapped to a concatenated genome sequence of human GRCh38/hg38 and mouse GRCm38/mm10 as previously described (14). The footprint plots were made with DeepTools2 (58).

Clustering ATAC-Seq Peaks. The DESeq2 (59) algorithm was used to identify differentially expressed peaks across all pairs of conditions, with a false discovery rate (FDR) threshold of 0.01. The resulting set of differential ATAC-seq peaks was clustered with the DPGP algorithm (22).

Motif Enrichment Analysis. Cluster-specific motif enrichment analysis was computed for 62 transcription factor motifs that had been identified from ChIP-seq datasets produced by the ENCODE Project in IMR90 fibroblast (ENCODE ID E017) and H1-hESC (ENCODE ID E003) cell lines (24).

Chromatin State Distributions. The 12-mark/127-reference epigenome/25-state imputation-based chromatin state model (60) from the Roadmap Epigenomics Project (23) was obtained from http://compbio.mit.edu/roadmap.

iPSC Generation and Propagation. MRC-5s (ATCC CCL-171) were transduced with dnAP-1 and expanded in media with tetracycline-free FBS (Clontech). Prior to reprogramming, they were treated with telomerase reverse transcriptase mmRNA as described (61). For iPSC reprogramming, 100,000 MRC-5s were seeded per well of a six-well plate with Geltrex (Thermo A1569601). The next day, cells were transduced using concentrated viral supernatant. The following day, media were changed to NutriStem (Reprocell 01-0005), with 30/70 (old-to-new ratio) daily media changes throughout the reprogramming process. The cells were kept at a 5% O_2 environment for the duration of the reprogramming process. For colony propagation, media were gradually changed to KO DMEM/F12, 20% knockout serum replacement, 10% conditioned media, nonessential amino acids, L-glutamine, 20 ng/mL basic fibroblast growth factor, 0.1 mM β-mercaptoethanol, and antibiotic. Colonies were picked onto irradiated feeders.

Chromatin Immunoprecipitation. For ChIPmentation, samples were processed in a tagmentation reaction, washed, and libraries were amplified and eluted as described previously (27, 62). qPCR was performed as described above using primers listed in *SI Appendix*, Table S5.

Data Availability. The sequencing data generated for this study are available on Gene Expression Omnibus under accession no. GSE121053 (63).

ACKNOWLEDGMENTS. We acknowledge the gracious aid of J. Buenrostro in the initial ATAC-seq experiments. We thank S. Corbel for advice and expertise, especially in FACS. We thank J. Brady for expertise in experimental procedures. We thank B. Hendrich for his kind contribution of the mouse ESC lines used in the PLA. We acknowledge M. Bassik for the contribution of the dCas9-KRAB plasmid, D. Bohmann for plasmids containing mutant forms of c-Jun, and R. Davis for the constitutive JNK expression plasmids. We acknowledge the resources of the Stanford Shared FACS Facility, FACS Core Facility in Stanford Lokey Stem Cell Research Building, the Stanford Protein and Nucleic Acid facility for oligo synthesis, and the Stanford Genomics core in this study. This research was supported by the T32 NIH training grant AG000266-20A1 (G.J.M.), NSF Graduate Research Fellowships Program DGE-1147470 (G.J.M.), F32 GM112425-02 (T.M.), Stanford Bio-X Fellowship (A.S.), Canadian Institutes of Health Research MFE-152457 grant (Y.X.W.), NIH grant RHG009674A (H.M.B. and A.K.), the Baxter Foundation (H.M.B.), and the Li Ka Shing Foundation (H.M.B.).

1. K. Takahashi, S. Yamanaka, Induction of pluripotent stem cells from mouse embryonic and adult fibroblast cultures by defined factors. *Cell* **126**, 663–676 (2006).
2. V. Tabar, L. Studer, Pluripotent stem cells in regenerative medicine: Challenges and recent progress. *Nat. Rev. Genet.* **15**, 82–92 (2014).
3. G. Tiscornia, E. L. Vivas, J. C. Izpisúa Belmonte, Diseases in a dish: Modeling human genetic disorders using induced pluripotent cells. *Nat. Med.* **17**, 1570–1576 (2011).
4. J. Wu, J. C. Izpisua Belmonte, Stem cells: A renaissance in human Biology research. *Cell* **165**, 1572–1585 (2016).
5. E. Apostolou, K. Hochedlinger, Chromatin dynamics during cellular reprogramming. *Nature* **502**, 462–471 (2013).
6. C. Chronis *et al*., Cooperative binding of transcription factors orchestrates reprogramming. *Cell* **168**, 442–459.e20 (2017).
7. A. Soufi, G. Donahue, K. S. Zaret, Facilitators and impediments of the pluripotency reprogramming factors' initial engagement with the genome. *Cell* **151**, 994–1004 (2012).
8. J. Hanna *et al*., Direct reprogramming of terminally differentiated mature B lymphocytes to pluripotency. *Cell* **133**, 250–264 (2008).
9. M. Mall *et al*., Myt1l safeguards neuronal identity by actively repressing many non-neuronal fates. *Nature* **544**, 245–249 (2017).
10. D. Li *et al*., Chromatin accessibility dynamics during iPSC reprogramming. *Cell Stem Cell* **21**, 819–833.e6 (2017).
11. H. M. Blau, C.-P. Chiu, C. Webster, Cytoplasmic activation of human nuclear genes in stable heterocaryons. *Cell* **32**, 1171–1180 (1983).
12. H. M. Blau *et al*., Plasticity of the differentiated state. *Science* **230**, 758–766 (1985).
13. N. Bhutani *et al*., Reprogramming towards pluripotency requires AID-dependent DNA demethylation. *Nature* **463**, 1042–1047 (2010).
14. T. Mai *et al*., NKX3-1 is required for induced pluripotent stem cell reprogramming and can replace OCT4 in mouse and human iPSC induction. *Nat. Cell Biol.* **20**, 900–908 (2018).
15. J. J. Brady *et al*., Early role for IL-6 signalling during generation of induced pluripotent stem cells revealed by heterokaryon RNA-Seq. *Nat. Cell Biol.* **15**, 1244–1252 (2013).
16. W. Lee, A. Haslinger, M. Karin, R. Tjian, Activation of transcription by two factors that bind promoter and enhancer sequences of the human metallothionein gene and SV40. *Nature* **325**, 368–372 (1987).
17. P. Angel, K. Hattori, T. Smeal, M. Karin, The jun proto-oncogene is positively autoregulated by its product, Jun/AP-1. *Cell* **55**, 875–885 (1988).
18. E. Shaulian, M. Karin, AP-1 in cell proliferation and survival. *Oncogene* **20**, 2390–2400 (2001).
19. Y. Rais *et al*., Deterministic direct reprogramming of somatic cells to pluripotency. *Nature* **502**, 65–70 (2013).
20. R. L. dos Santos *et al*., MBD3/NuRD facilitates induction of pluripotency in a context-dependent manner. *Cell Stem Cell* **15**, 102–110 (2014).
21. J. Liu *et al*., The oncogene c-Jun impedes somatic cell reprogramming. *Nat. Cell Biol.* **17**, 856–867 (2015).
22. I. C. McDowell *et al*., Clustering gene expression time series data using an infinite Gaussian process mixture model. *PLoS Comput. Biol.* **14**, e1005896 (2018).
23. A. Kundaje *et al*.; Roadmap Epigenomics Consortium, Integrative analysis of 111 reference human epigenomes. *Nature* **518**, 317–330 (2015).
24. P. Kheradpour, M. Kellis, Systematic discovery and characterization of regulatory motifs in ENCODE TF binding experiments. *Nucleic Acids Res.* **42**, 2976–2987 (2014).
25. R. Eferl, E. F. Wagner, AP-1: A double-edged sword in tumorigenesis. *Nat. Rev. Cancer* **3**, 859–868 (2003).
26. T. D. Halazonetis, K. Georgopoulos, M. E. Greenberg, P. Leder, c-Jun dimerizes with itself and with c-Fos, forming complexes of different DNA binding affinities. *Cell* **55**, 917–924 (1988).
27. C. Gustafsson, A. De Paepe, C. Schmidl, R. Månsson, High-throughput ChIPmentation: Freely scalable, single day ChIPseq data generation from very low cell-numbers. *BMC Genomics* **20**, 59 (2019).
28. C. J. Gröger, M. Grubinger, T. Waldhör, K. Vierlinger, W. Mikulits, Meta-analysis of gene expression signatures defining the epithelial to mesenchymal transition during cancer progression. *PLoS One* **7**, e51136 (2012).
29. X. Fang *et al*., Twist2 contributes to breast cancer progression by promoting an epithelial-mesenchymal transition and cancer stem-like cell self-renewal. *Oncogene* **30**, 4707–4720 (2011).
30. J. J. Rodgers *et al*.; Australian Prostate Cancer BioResource, ETS1 induces transforming growth factor β signaling and promotes epithelial-to-mesenchymal transition in prostate cancer cells. *J. Cell. Biochem.* **120**, 848–860 (2019).
31. C. Y. McLean *et al*., GREAT improves functional interpretation of cis-regulatory regions. *Nat. Biotechnol.* **28**, 495–501 (2010).
32. M. Olive *et al*., A dominant negative to activation protein-1 (AP1) that abolishes DNA binding and inhibits oncogenesis. *J. Biol. Chem.* **272**, 18586–18594 (1997).
33. J. Zhang *et al*., LIN28 regulates stem cell metabolism and conversion to primed pluripotency. *Cell Stem Cell* **19**, 66–80 (2016).
34. J. S. You *et al*., OCT4 establishes and maintains nucleosome-depleted regions that provide additional layers of epigenetic regulation of its target genes. *Proc. Natl. Acad. Sci. U.S.A.* **108**, 14497–14502 (2011).
35. D. J. Rodda *et al*., Transcriptional regulation of nanog by OCT4 and SOX2. *J. Biol. Chem.* **280**, 24731–24737 (2005).
36. P. I. Thakore *et al*., Highly specific epigenome editing by CRISPR-Cas9 repressors for silencing of distal regulatory elements. *Nat. Methods* **12**, 1143–1149 (2015).
37. N. A. Kearns *et al*., Functional annotation of native enhancers with a Cas9-histone demethylase fusion. *Nat. Methods* **12**, 401–403 (2015).
38. C. B. Ware *et al*., Derivation of naive human embryonic stem cells. *Proc. Natl. Acad. Sci. U.S.A.* **111**, 4484–4489 (2014).
39. L. S. Qi *et al*., Repurposing CRISPR as an RNA-guided platform for sequence-specific control of gene expression. *Cell* **152**, 1173–1183 (2013).
40. B.-K. Chen, W.-C. Chang, Functional interaction between c-Jun and promoter factor Sp1 in epidermal growth factor-induced gene expression of human 12(S)-lipoxygenase. *Proc. Natl. Acad. Sci. U.S.A.* **97**, 10406–10411 (2000).
41. C. Aguilera *et al*., c-Jun N-terminal phosphorylation antagonises recruitment of the Mbd3/NuRD repressor complex. *Nature* **469**, 231–235 (2011).
42. S. Bornelöv *et al*., The nucleosome remodeling and deacetylation complex modulates chromatin structure at sites of active transcription to fine-tune gene expression. *Mol. Cell* **71**, 56–72.e4 (2018).
43. K. Lei *et al*., The Bax subfamily of Bcl2-related proteins is essential for apoptotic signal transduction by c-Jun NH(2)-terminal kinase. *Mol. Cell. Biol.* **22**, 4929–4942 (2002).
44. B. Dérijard *et al*., JNK1: A protein kinase stimulated by UV light and Ha-Ras that binds and phosphorylates the c-Jun activation domain. *Cell* **76**, 1025–1037 (1994).
45. C. Tournier, A. J. Whitmarsh, J. Cavanagh, T. Barrett, R. J. Davis, The MKK7 gene encodes a group of c-Jun NH2-terminal kinase kinases. *Mol. Cell. Biol.* **19**, 1569–1581 (1999).
46. A. M. Musti, M. Treier, D. Bohmann, Reduced ubiquitin-dependent degradation of c-Jun after phosphorylation by MAP kinases. *Science* **275**, 400–402 (1997).
47. M. Wernig, A. Meissner, J. P. Cassady, R. Jaenisch, c-Myc is dispensable for direct reprogramming of mouse fibroblasts. *Cell Stem Cell* **2**, 10–12 (2008).
48. J. Chen *et al*., H3K9 methylation is a barrier during somatic cell reprogramming into iPSCs. *Nat. Genet.* **45**, 34–42 (2013).
49. S. Hu *et al*., Effects of cellular origin on differentiation of human induced pluripotent stem cell-derived endothelial cells. *JCI Insight* **1**, e85558 (2016).
50. J.-H. Lee *et al*., Somatic transcriptome priming gates lineage-specific differentiation potential of human-induced pluripotent stem cell states. *Nat. Commun.* **5**, 5605 (2014).
51. L. Cui *et al*., Activation of JUN in fibroblasts promotes pro-fibrotic programme and modulates protective immunity. *Nat. Commun.* **11**, 2795 (2020).
52. G. Wernig *et al*., Unifying mechanism for different fibrotic diseases. *Proc. Natl. Acad. Sci. U.S.A.* **114**, 4757–4762 (2017).
53. T. Vierbuchen *et al*., AP-1 transcription factors and the BAF complex mediate signal-dependent enhancer selection. *Mol. Cell* **68**, 1067–1082.e12 (2017).
54. M. Luo *et al*., NuRD blocks reprogramming of mouse somatic cells into pluripotent stem cells. *Stem Cells* **31**, 1278–1286 (2013).
55. A. MacLaren, E. J. Black, W. Clark, D. A. F. Gillespie, c-Jun-deficient cells undergo premature senescence as a result of spontaneous DNA damage accumulation. *Mol. Cell. Biol.* **24**, 9006–9018 (2004).
56. J. D. Hoeck *et al*., Fbw7 controls neural stem cell differentiation and progenitor apoptosis via Notch and c-Jun. *Nat. Neurosci.* **13**, 1365–1372 (2010).
57. R. Li *et al*., MBD3 inhibits formation of liver cancer stem cells. *Oncotarget* **8**, 6067–6078 (2017).
58. F. Ramírez *et al*., deepTools2: A next generation web server for deep-sequencing data analysis. *Nucleic Acids Res.* **44**, W160–W165 (2016).
59. M. I. Love, W. Huber, S. Anders, Moderated estimation of fold change and dispersion for RNA-seq data with DESeq2. *Genome Biol.* **15**, 550 (2014).
60. J. Ernst, M. Kellis, ChromHMM: Automating chromatin-state discovery and characterization. *Nat. Methods* **9**, 215–216 (2012).
61. J. Ramunas *et al*., Transient delivery of modified mRNA encoding TERT rapidly extends telomeres in human cells. *FASEB J.* **29**, 1930–1939 (2015).
62. C. Schmidl, A. F. Rendeiro, N. C. Sheffield, C. Bock, ChIPmentation: Fast, robust, low-input ChIP-seq for histones and transcription factors. *Nat. Methods* **12**, 963–965 (2015).
63. G. Markov *et al*., AP-1 is a temporally regulated dual gatekeeper of reprogramming to pluripotency. *Gene Expression Omnibus*. https://www.ncbi.nlm.nih.gov/geo/query/acc.cgi?acc=GSE121053. Deposited 21 May 2021.